A numerical forecast of fluid motion in a rotating tank and a study of how finite-difference approximations affect non-linear interactions

By HILDING SUNDQVIST, *Institute of Meteorology, University of Stockholm*

(Manuscript received November 8, 1962; revised version February 5, 1963)

ABSTRACT

Using observational data of the fluid motion in a laboratory experiment with a rotating tank numerical forecasts with three different models were made. The Ekman friction was taken into account. The forecasts were verified statistically and the results for the different models were compared.

An investigation of the effect of observational errors was made and it was found that errors in the initial field do not affect the prediction severely.

The spectral distribution of kinetic energy in the forecast data and the verification data were compared. Systematic differences between observed and forecast distributions stimulated a study of the effect of finite differences on non-linear interactions. A theoretical discussion shows that when finite differences are applied to the non-linear vorticity equation a leakage of energy from the long waves to the shortest ones occurs.

To test this conclusion a numerical forecast was made with three different grid intervals, as well as a forecast of the Fourier components of the field of motion.

Finally, it is discussed how the fictitious flow of energy may give rise to the special kind of computational instability that Phillips has investigated.

1. Introduction

When checking numerical weather forecasts against observations it is usually very difficult to trace the errors back to their origin. Errors may be due to simplifications in the hydro-thermodynamic equations, observational errors or pure numerical effects.

If the basic equations are applied to a physically simpler system the difficulty mentioned above is partly avoided. The errors appearing in a forecast of this system could with greater certainty be ascribed to definite causes. Such a physically simple system can be produced in a laboratory experiment using a rotating tank containing water of constant temperature. Thus one is concerned with the motion of a homogeneous fluid. The present paper describes a first attempt to make numerical forecasts based on data obtained from such experiments. The results of forecasts with three different models will be presented. The influence of observational errors and certain aspects of the spectral distribution of kinetic energy are discussed. Finally, a detailed study of the effects of finite-difference approximations will be made.

2. The models

Considering a homogeneous and incompressible fluid whose motion is essentially horizontal and is in quasi-geostrophic balance we apply the vorticity equation:

$$\frac{\partial \zeta}{\partial t} = -\mathbf{v} \cdot \nabla \zeta - (\zeta + f)\, \nabla \cdot \mathbf{v}. \qquad (1)$$

f, the Coriolis parameter, is constant in the tank;
$\mathbf{v}$ is the horizontal wind vector;
ζ is the vertical component of the vorticity; and
∇ is the horizontal del-operator.

Lateral friction is omitted since, as is shown below, for the scales of motion considered here, lateral friction is unimportant compared with bottom friction.

Bottom friction and vertical motions at the free surface of the fluid generate horizontal divergence. Because the fluid is homogeneous and in quasi-geostrophic balance $\mathbf{v}$ is independent of height between the top of the friction layer and the free surface. After integration of the continuity equation with respect to z one finds

$$\nabla \cdot \mathbf{v} = -\frac{w_2 - w_1}{H + h - z_g},$$

where H is the depth of the water at relative rest, h is the height perturbation due to relative motions in the tank, z_g is the depth of the friction layer and w_1, and w_2 are the vertical velocities at z_g and $H+h$ respectively. The assumption that a particle at the surface always stays there, gives $w_2 = (d/dt)\ (H+h)$. In order to get an expression for w_1, we apply the Ekman theory (EKMAN, 1905) to the friction layer as is done by CHARNEY and ELIASSEN (1949):

Thus $$w_1 = A\zeta,$$

where $A = \sqrt{\nu/2f}$ and ν is the kinematic viscosity.

Before the expressions for w_1 and w_2 are inserted a simplification of the denominator $(H+h-z_g)$ will be made. When the fluid is at relative rest the free surface has the shape of a paraboloid. The radial variation of H is

$$H = H_0 + \frac{r^2 f^2}{8g}. \tag{2}$$

H_0 is the depth at the center, r is the radius and g is the acceleration due to gravity. If H is put equal to the depth measured at absolute rest, it deviates with only one or two per cent from its true value, because the rotation is slow. The relative flow in the vessel is such that even h can change the denominator by only one or two per cent. Therefore, in the following the denominator will be regarded as a constant and written $(H - z_g)$, where H means the depth of the water at absolute rest.

Hence we may rewrite equation (1) as

$$\frac{\partial \zeta}{\partial t} = -\mathbf{v} \cdot \nabla \zeta - \frac{\zeta + f}{H - z_g}\left[A\zeta - \frac{d}{dt}(H+h)\right]. \tag{3}$$

The first term in square brackets shows that the effect of bottom friction always is to decrease the relative vorticity of the fluid.

The second term in square brackets, $dH/dt = \mathbf{v}\cdot\nabla H$ (since $\partial H/\partial t = 0$) increases or decreases the relative vorticity depending upon whether the flow has a component directed away from or towards the center of rotation. This is caused by the convergence (divergence), which a column of fluid experiences when it moves in the direction of increasing (decreasing) depth. From this we see that the term $\mathbf{v}\cdot\nabla H$ has the same effect as the β-term in the atmosphere. Therefore, in the following $\mathbf{v}\cdot\nabla H$ will be called the β-term.

In order to utilize equation (3) as it stands it is necessary to have another expression which determines the relationships between the height field h, and the wind field (e.g. the balance eq., see BOLIN, (1955, 1956).

However, from the insertion of actual values from the experiments and by scale considerations it can be shown that

(a) $|A\zeta| \sim 10 \cdot |\mathbf{v}\cdot\nabla H|$,

(b) $|A\zeta| \sim 10^2 |\mathbf{v}\cdot\nabla h| - 10^3 |\mathbf{v}\cdot\nabla h|$,

(c) $|A\zeta| \sim 10 \left|\frac{\partial h}{\partial t}\right|$.

In this connection it should be mentioned that z_g in the denominator in equation (3) was omitted in the computations to be presented here. Thus, we have a somewhat smaller influence (about 10%) by the divergence term than there should be.

With the estimates stated above, as a background, three forecasting models were deduced from equation (3). In all three the two terms $\partial h/\partial t$ and $\mathbf{v}\cdot\nabla h$ were omitted. The possibility that the local change $\partial h/\partial t$ may play some role in some areas of the field should be kept in mind during the consideration of the results. The three models are as follows.

Model I

The advection of vorticity by the divergent part of the wind, $\mathbf{v}_D\cdot\nabla\zeta$, the divergence term depending on relative vorticity $\zeta\nabla\cdot\mathbf{v}$ and the β-term were neglected in this model. The stream function was introduced. Accordingly we have

$$\frac{\partial}{\partial t}\nabla^2\psi = -J(\psi, \nabla^2\psi) - D\cdot\nabla^2\psi, \tag{4}$$

where J as usual denotes the Jacobian and $D = Af/(H - z_g) \simeq Af/H$.

Model II

This is an extension of Model I in that the two terms $\mathbf{v}_D\cdot\nabla\zeta$ and $\zeta\nabla\cdot\mathbf{v}$ are included. This inclusion is easily accomplished since,

$$\nabla\cdot\mathbf{v} = \frac{A}{H}\zeta = \frac{A}{H}\nabla^2\psi$$

because the terms $\mathbf{v}\cdot\nabla H$, $\partial h/\partial t$ and $\mathbf{v}\cdot\nabla h$ are omitted. Thus the divergent part of the wind can be expressed as $(A/H)\nabla\psi$. Hence we still have the stream function as the only unknown to predict:

$$\frac{\partial}{\partial t}\nabla^2\psi = -J(\psi, \nabla^2\psi) - \frac{A}{H}\nabla\psi\cdot\nabla(\nabla^2\psi)$$

$$-\frac{\nabla^2\psi + f}{H}A\nabla^2\psi. \tag{5}$$

Model III

This model is also an extension of Model I, in the respect that the β-term is retained. This third model was derived after having compared forecasts made with Models I and II. This comparison showed that there was a well-marked balance between the terms $\mathbf{v}_D\cdot\nabla\zeta$ and $\zeta\nabla\cdot\mathbf{v}$. The β-term was therefore added to Model I, the simpler but equally accurate model.

From expression (2) we get

$$\frac{\partial H}{\partial x} = \frac{f^2}{4g}(x-a) \quad\text{and}\quad \frac{\partial H}{\partial y} = \frac{f^2}{4g}(y-a),$$

where $(a; a)$ are the coordinates for the center of the vessel. So Model III was

$$\frac{\partial}{\partial t}\nabla^2\psi = -J(\psi, \nabla^2\psi) - D\cdot\nabla^2\psi$$

$$-\frac{f^3}{4gH}\left[(x-a)\frac{\partial\psi}{\partial y} - (y-a)\frac{\partial\psi}{\partial x}\right]. \tag{6}$$

A short description of the computation methods is found in the Appendix.

In order to solve numerically the equations derived above it is necessary to prescribe both $\partial\psi/\partial t$ and $\nabla^2\psi$ on the boundary; the latter condition making it possible to evaluate the Jacobian at points next to the boundary. The boundary conditions that were applied were:

$$\left.\begin{aligned}&(a)\ \ \psi \equiv 0\\ &(b)\ \ \zeta = \nabla^2\psi \equiv 0\end{aligned}\right\}\quad\text{along the walls.}$$

Condition (a) excludes normal velocities at the walls at all times. In order to evaluate ζ at the walls one must know ψ at points outside the walls. Now ψ is prescribed at these points by linearly extrapolating ψ from the points on the walls and the nearest points inside the walls. This can be expressed by the requirement (b), because $\psi \equiv 0$ along the walls.

3. Experimental procedure

The experiments were carried out at a slow rotation rate. Furthermore a small Rossby number was aimed at. In the case to be discussed here the rotation rate was about 0.5 radians sec^{-1} and the maximum relative speed about 3 cm sec^{-1}. The fluid depth was approximately 7 cm. The experimental procedure was as follows.

In order to get a grid system for the numerical integration easily fitted to the geometry of the tank, a square tank was chosen (92×92 cm). The inner sides of the walls were covered with a porous material for the purpose of damping gravity waves.

Relative motions were obtained by means of a camera which rotated with the vessel and which automatically took one time exposure per revolution. Fig. 1 shows the resultant streaks caused by paper discs on the water surface. On the rotating table there were contacts which first opened the camera shutter then triggered one of the flashes. When the table had turned 30 degrees more both flashes were triggered at the same time and the camera shutter closed. In this way weak streaks with two points of different light intensity were obtained so that the velocity of each moving disc could be measured.

To produce an initial circulation the tank was first rotated until the whole mass of water was at relative rest. Then an irregular metal frame in the center of the tank was gently twisted, the frame was removed, and the initial fluid

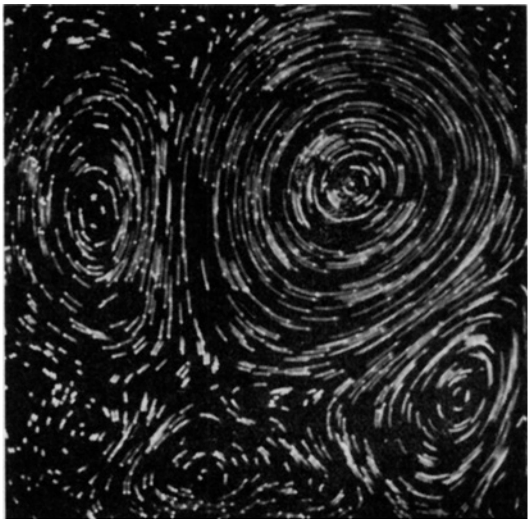

FIG. 1. A streak photograph illustrating the method for obtaining the fluid velocity.

motion was photographed. An example of the resulting motion is shown in Fig. 1.

The pictures were projected on a sheet of millimeter paper which was 1 meter square. The scales of motion were such that it seemed reasonable to use a 20×20 grid with a spacing of 5 cm on the enlarged projection. Streamlines were drawn following the streaks of the projected image, and the magnitudes of the velocity vectors were estimated from the neighboring streaks. The vectors were then easily resolved into their x and y components from the millimeter paper.

Since the number of streaks was considerably larger than the number of grid points, the coverage of the data for the numerical treatment was relatively good. The standard deviation of the errors of observation of the velocity components was determined statistically from the requirement of continuity of flow across any section and was found to be about 8% of the mean speeds.

4. Results of forecasting with the various models

The quantities that are commonly used in verification of numerical weather forecasts were also used in this case:

$$\bar{x} = \overline{\psi^{\tau}_{\text{obs}} - \psi^{\circ}}, \quad \bar{y} = \overline{\psi^{\tau}_{\text{pr}} - \psi^{\circ}}, \quad \sigma_x = \sqrt{\bar{x}^2},$$

$$\sigma_y = \sqrt{\bar{y}^2}, \quad \varepsilon = \sqrt{(\bar{x} - \bar{y})^2}, \quad \varepsilon/\sigma_x, \quad r.$$

The bar denotes the average over the area under consideration. τ denotes the number of revolutions. (For convenience one revolution will be called one day in the following.) Thus x and y give respectively the observed and the predicted changes of ψ from the initial field up to τ days. ε is the RMS error of the predicted changes and ε/σ_x is the relative error. r is the correlation coefficient between x and y. Of course these verification quantities only give an average picture of how successful the predictions have been. Still they give some information on differences between the prognostic models.

Table 1 shows the values obtained for the above mentioned parameters. (The results for three days are, for the sake of brevity, not shown because they possess the very same features as for the other days.) The area of verification was a square with its boundaries at a distance of three grid intervals from the walls. In this way the area of verification extends over the greater part of the field of motion, but does not come too near the walls (see Figs. 2–6). Since $\psi \equiv 0$ at the walls both in the forecast and in the observations, a verification even of the excluded region would not be very meaningful.

TABLE 1.

			$\bar{y}$			σ_y			ε/σ_x			r		
τ	$\bar{x}$	σ_x	Mod. I	Mod. II	Mod. III	Mod. I	Mod. II	Mod. III	Mod. I	Mod. II	Mod. III	Mod. I	Mod. II	Mod. III
1	−1.54	5.94	−1.62	−1.18	−1.64	5.03	4.95	5.30	0.260	0.264	0.223	0.949	0.951	0.965
2	−2.36	9.17	−2.51	−1.67	−2.45	7.86	7.76	8.29	0.268	0.279	0.221	0.952	0.952	0.969
4	−2.75	11.21	−3.63	−2.08	−2.99	10.62	10.59	10.96	0.287	0.283	0.228	0.953	0.956	0.971

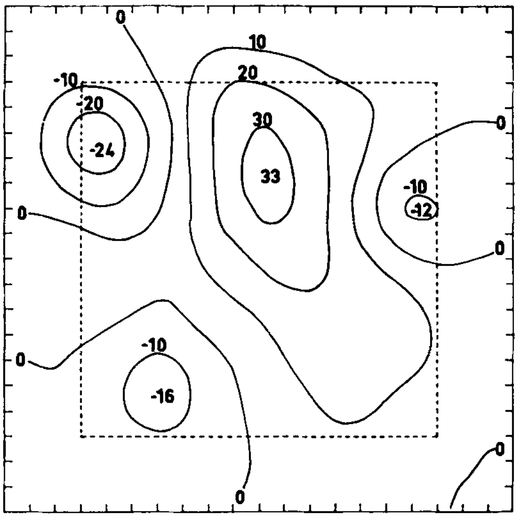

FIG. 2. Initial field for the forecasts. Full lines are isopleths for the streamfunction. (Unit $cm^2 sec^{-1}$). Dashed lines are the boundaries for the verification area.

That the forecasts were so successful as shown by Table I might to some extent depend upon the fact that the wave pattern was almost stationary. (Compare Figs. 2 and 3.)

A notable point is that the forecast over four days was as good as that over one day. This fact indicates that no spurious boundary effects due to boundary condition (*b*) have been advected into the region of verification. The absence of

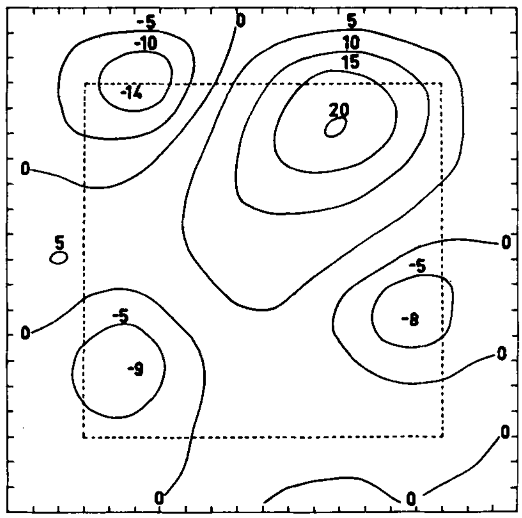

FIG. 4. Four-day forecast according to Model I.

distortion by boundary effects can be explained by the fact that we have a well-defined system across whose boundaries no advection occurs. The constancy or slight increase of r will be discussed further in connection with the effects of observational errors.

From a comparison of Models I and II we gather that they give almost identical average results. This implies that there exists a balance between the two terms $\mathbf{v}_D \cdot \nabla \zeta$ and $\zeta \nabla \cdot \mathbf{v}$. A careful comparison of the predicted fields obtained from Models I and II did indeed reveal

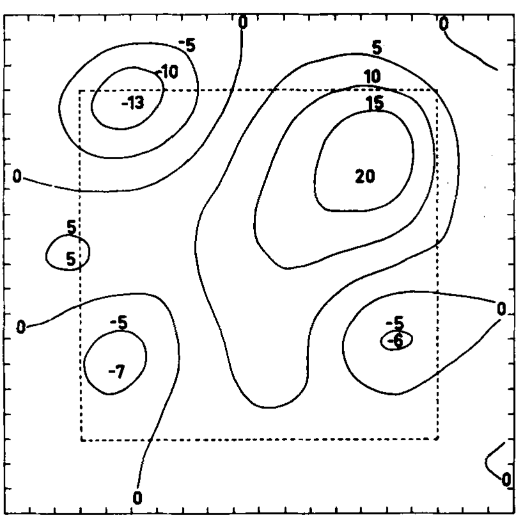

FIG. 3. Observed field four days after that shown in Fig. 2.

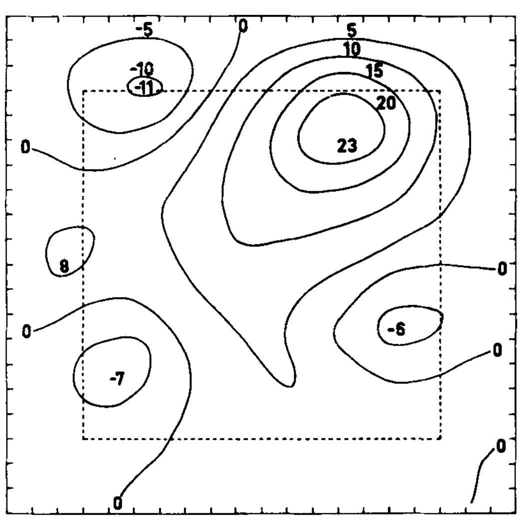

FIG. 5. Four-day forecast according to Model II.

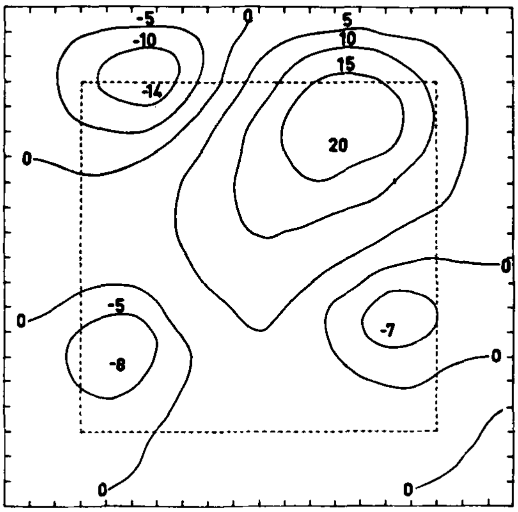

FIG. 6. Four-day forecast according to Model III.

a well-established balance between these two terms, except near vorticity maxima and minima. (Those facts can to some extent be seen in Figs. 4 and 5.) Around these maxima and minima the advection term becomes very small or zero, because of the disappearance of $\nabla\zeta$, while the term $\zeta\nabla\cdot\mathbf{v}$ has its greatest influence. Thus we cannot expect a balance in those regions. If, in addition, z_g had been included (necessary, as will be shown later, in order to give a correct decay of kinetic energy), the effects from $\zeta\nabla\cdot\mathbf{v}$ would have been still more pronounced at the extreme points of vorticity. Thus it could be concluded from the forecast fields that the forecasts by Model II would not have been as good as the forecasts by Model I. This means that if we want to retain the terms $\mathbf{v}_D\cdot\nabla\zeta$ and $\zeta\nabla\cdot\mathbf{v}$ which on the whole are of smaller order of magnitude than the leading terms, then we probably have to take all other neglected terms of the same order of magnitude into account at the same time.

We also come to the same conclusion if we consider the term $\partial h/\partial t$ alone. Since we have a quasi-stationary situation it is possible to carry through a qualitative discussion of the term. The motion of the fluid will gradually be damped out by the friction and by virtue of the stationary condition we are able to say that $\partial h/\partial t$ will not change sign, except for a few points, during the prognostic period. Consequently $\partial h/\partial t$ is positive in the cyclonic areas and negative in the anticyclonic areas. Hence we see from equation (3) that the absolute value of the divergence term—that is, the friction term—becomes reduced if $\partial h/\partial t$ is included. From Figs. 3 and 4 we see that the cyclones have become somewhat too deep in the forecast and that there is at least a tendency for the anticyclone to be too high. If $\partial h/\partial t$ alone had been taken into account, these deviations would have been still more conspicuous.

Let us go back to Table I and look at the results for Model III. These show that a distinct improvement of the forecast is obtained by applying Model III instead of either Model I or Model II. (See also Fig. 6.) This is also in agreement with the estimates made before, in which the β-term appeared to be the most important one of the terms omitted. According to what was said in the former section about retaining all terms of the same order of magnitude it may seem paradoxical that the inclusion of this single term of the smaller ones results in improvement of the forecast. However, the β-term is not directly connected with the other omitted terms, but originates from the geometry of the system.

Observational errors

In order to see how observational errors affect the accuracy of the forecasts, additional errors were introduced into each of the observed velocity fields. Then a new forecast was made by Model I and the verification parameters were computed.

In the hope of getting significant changes in the fields it was decided that the standard deviation of the new observational errors of the velocity vectors should be twice the standard deviation of the original errors. As mentioned earlier the latter was estimated to be about 8%. Accordingly, it was easy to compute what the additional errors should be since they were assumed to be normally distributed around zero per cent with a maximum of ± 25 per cent. (See Appendix.) At each point both the x component and the y component were randomly given the same error, that is, only the magnitude of the wind vector was changed.

The results, obtained when the new forecasts were verified against the new fields of observational data are shown in Table 2a. In Table 2b we find the results obtained when the same

TABLE 2.

	τ	$\bar{x}$	σ_x	$\bar{y}$	σ_y	ε/σ_x	r
(a)	1	−2.84	7.70	−1.69	5.34	0.460	0.835
	2	−2.15	9.96	−2.53	8.28	0.373	0.908
	4	−2.82	11.44	−3.32	10.97	0.272	0.958
(b)	1	−1.54	5.94	−1.53	5.15	0.261	0.950
	2	−2.36	9.17	−2.37	8.06	0.264	0.954
	4	−2.75	11.21	−3.16	10.70	0.279	0.955

forecasts were verified against the originally observed fields.

Table 2*a* gives the impression that the forecast over one day is not as accurate as those over two and four days. But from Table 2*b* one sees that the forecasts have the same accuracy as before (Table 1). Hence the major reason for obtaining worse values of the parameters in Table 2*a* is that the forecasts have been verified against less accurate observation fields. *Thus the observation errors in the initial field seem to have a very small effect on the accuracy of a forecast (at least in a system without any sources of energy); the ostensible failure as shown by statistical quantities rather depends in part upon the inaccuracies in the field against which the forecast is verified.*

As becomes quite evident in Table 2*a*, there is a systematic increase of r with increasing prognostic time. This phenomenon can be explained by the following consideration. Let us assume that we have a perfect forecasting equation. Then the only errors that will appear in the forecast are those that originate from the observational errors in the initial field. So we write for the observed and predicted changes respectively

$$x = \psi^\tau - \psi^\circ + \varepsilon^\tau_{\text{obs}} - \varepsilon^\circ_{\text{obs}},$$

$$y = \psi^\tau - \psi^\circ + \varepsilon^\tau_{\text{pr}} - \varepsilon^\circ_{\text{obs}},$$

where ψ is the true value of the stream function, ε_{obs} are the observational errors, and ε_{pr} are the errors in the forecast. Further we assume the errors to be random. That is

$$\bar{x} = \bar{y} = \overline{\psi^\tau - \psi^\circ}.$$

Then we find from the definition of r:

$$r^2 = \frac{\overline{(x-\bar{x})\cdot(y-\bar{y})}^2}{\overline{(x-\bar{x})^2}\cdot\overline{(y-\bar{y})^2}} = \frac{(A+\overline{\varepsilon_{\text{pr}}\cdot\Delta^\tau})^2}{A^2+A\cdot B},$$

where

$$\Delta^\tau = \psi^\tau - \psi^\circ,$$

$$A = \overline{(\Delta^\tau)^2} - \overline{\Delta^\tau}^2,$$

$$B = \overline{(\varepsilon^\tau_{\text{obs}} - \varepsilon^\circ_{\text{obs}})^2} + \overline{(\varepsilon^\tau_{\text{pr}} - \varepsilon^\circ_{\text{obs}})^2}.$$

The covariance $|\overline{\varepsilon_{\text{pr}}\cdot\Delta^\tau}|$ may have a value different from zero, but it can probably be neglected in comparison with A and thus

$$r^2 = \frac{1}{1+B/A}.$$

Since we know that the field of motion is being damped due to frictional effects we can conclude that A increases with time. This statement is verified by a glance at the values for $\bar{x}$ and σ_x in Table 1 or Table 2. Furthermore, B probably does not increase as fast as A does. That is to say, r will increase with time. In addition we see from this consideration why r starts with a higher value in Table 2*b* than in Table 2*a*. If we regard the original fields as being exact, we have $B = \overline{(\varepsilon^\tau_{\text{pr}})^2}$ when computing r in Table 2*b*. This value of B is less than in case II*a* where

$$B = 2\overline{(\varepsilon^\circ_{\text{obs}})^2} + \overline{(\varepsilon^\tau_{\text{obs}})^2} + \overline{(\varepsilon^\tau_{\text{pr}})^2}.$$

On Fourier analysis and spectral distribution of the kinetic energy

In order to study the distribution and transfer of kinetic energy in wave-number space, the stream function was expanded in a two-dimensional Fourier series. The Fourier analysis was applied to all the observation fields and to the forecast fields obtained from Model I. Model I was chosen because it is the simplest one in which the nonlinear term is retained through which a first attempt to predict the Fourier components could be made.

In order to satisfy the boundary condition (*a*), ψ is expanded in a sine series. This representation automatically gives $\nabla^2\psi \equiv 0$ along the walls. Thus we may write:

$$\psi = \sum_{m=1}^{N-1}\sum_{n=1}^{N-1} B_{mn} \sin\frac{m\pi x}{L} \sin\frac{n\pi y}{L} \qquad (7)$$

or

$$B_{mn} = \frac{4}{L^2} \int_0^L \int_0^L \psi(x, y) \sin \frac{m\pi x}{L} \sin \frac{n\pi y}{L} dx\,dy.$$

The integers m and n give the number of half waves over L in x and y directions respectively. L is the length of one side of the square region (tank). Since a grid system cannot discover wave lengths $< 2\Delta S$, only wavelengths $\geqslant 2\Delta S$ are considered in this expansion. Therefore we have

$$N = \frac{L}{\Delta s} \quad (= 20 \text{ for the cases presented here}).$$

Inserting (7) in the equation for Model I and utilizing orthogonality properties we find

$$\frac{d}{dt} B_{mn} = \frac{\pi^2}{4L^2(m^2+n^2)} \sum_{p=m-(N-1)}^{N-1} \sum_{q=n-(N-1)}^{N-1} \times \left\{ \varepsilon(np-mq)(p^2+q^2) B_{|p||q|} B_{|m-p||n-q|} \right\} - -D \cdot B_{mn} \tag{8}$$

where

$$\varepsilon = \begin{cases} +1 \begin{cases} \text{if} & p \cdot q > 0 & \text{and} & (m-p)\cdot(n-q) > 0 \\ \text{or} & p \cdot q < 0 & \text{and} & (m-p)\cdot(n-q) < 0 \end{cases} \\ -1 \begin{cases} \text{if} & p \cdot q < 0 & \text{and} & (m-p)\cdot(n-q) > 0 \\ \text{or} & p \cdot q > 0 & \text{and} & (m-p)\cdot(n-q) < 0 \end{cases} \end{cases}$$

The total kinetic energy K in the region expressed in terms of B_{mn} is

$$K = -\tfrac{1}{2} \int \psi \nabla^2 \psi dA = \frac{\pi^2}{8} \sum_{m=1}^{N-1} \sum_{n=1}^{N-1} (m^2+n^2) B_{mn}^2 \tag{9}$$

and the kinetic energy in wave-number $(m; n)$ is thus

$$K_{mn} = \frac{\pi^2}{8} (m^2+n^2) B_{mn}^2. \tag{10}$$

The time derivative of K_{mn} is now found by multiplying equation (8) by $\frac{1}{8}\pi^2(m^2+n^2) B_{mn}$:

$$\frac{d}{dt} K_{mn} = \frac{\pi^4}{16L^2} \sum_{p=m-(N-1)}^{N-1} \sum_{q=n-(N-1)}^{N-1} \times \left\{ \varepsilon(np-mq)(p^2+q^2) B_{mn} B_{|p||q|} B_{|m-p||n-q|} \right\} - 2D \cdot K_{mn}. \tag{11}$$

These equations have been derived and applied to the discussion of energy transfer in the wave number space by several authors, e.g. FJÖRTOFT (1953), LORENZ (1960) and SALTZMAN (1959).

Summation over m and n in (11) gives the rate of change of the total kinetic energy

$$\frac{dK}{dt} = -2D \cdot K \tag{12a}$$

or

$$K = K^\circ e^{-2D\cdot t}. \tag{12b}$$

For the purpose of studying the changes in K_{mn} which are due to non-linear interactions alone, we put $K_{mn}/K = P_{mn}$.

Inserting this into equation (11) we get

$$\frac{d}{dt} P_{mn} = \frac{\pi^4}{16L^2} \cdot \frac{1}{K} \sum_{p=m-(N-1)}^{N-1} \sum_{q=n-(N-1)}^{N-1} + \varepsilon(np-mq)(p^2+q^2) B_{mn} B_{|p||q|} B_{|m-p||n-q|}. \tag{13}$$

Equation (13) shows that the changes in the percentage distribution of kinetic energy within the spectrum are due only to the non-linear interactions. This is because lateral friction is omitted and bottom friction damps all waves at the same rate.

The total kinetic energy K in each of the fields was calculated in two ways. First the energy was computed directly from the observed velocity components (K_c) and with the aid of (12b) a prediction was made. Second, K was computed in both the observed and the forecast fields according to formula (9) (called K_F).

Table 3a shows K_c and K_F and the errors $K_{c\text{pr}}$ in arbitrary units. (The errors have almost the same values when comparing $K_{F\text{Ir}}$ and $K_{F\text{ct}}$). We see that the error increases with time. This is due to neglecting z_g in the computations. If the depth of the friction layer had been taken into account the error would have re-

TABLE 3.

	τ	K_c Obs.	K_c Prog.	K_c Error %	K_F Obs.	K_F Prog.		$K_{F\text{pr}}$ Analytic
(a)	0	289.5			260.4			
	1	207.4	217.4	+5	187.3	193.4	(b)	195.8
	2	147.9	163.4	+10	133.7	146.3		147.2
	4	80.1	92.5	+16	71.7	83.6		83.3

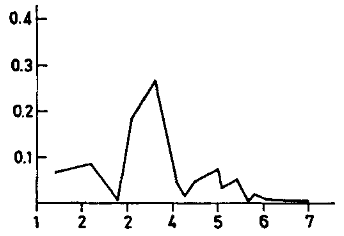

FIG. 7*a*. Observed distribution of $\Sigma P_{m,n}$ as defined in the text. Abscissa: $\sqrt{m^2+n^2}$.

mained rather small ($\leqslant 5\%$) throughout the prognostic time.

One may also think of the neglect of lateral friction as being responsible for the errors in the predicted energy. In order to get an idea about the influence of the lateral friction one can consider one Fourier component of ζ:

$$\zeta = A_{mn} \sin \frac{m\pi x}{L} \sin \frac{n\pi y}{L},$$

and take the ratio between the lateral friction term, $\nu\nabla^2\zeta$ and the bottom friction term, $D\cdot\zeta$. Hence one finds:

$$R_{mn}\left(\frac{\text{lateral frict.}}{\text{bottom frict.}}\right) = \frac{\pi^2(m^2+n^2)}{L\cdot\dfrac{Af}{H}}. \tag{14}$$

For the actual values in the experiment

$$R_{mn} \simeq 1.6\cdot 10^{-3}\,(m^2+n^2)$$

which gives e.g.

$$R_{5,5} \simeq 0.08, \quad R_{10,10} \simeq 0.33, \quad R_{19,19} \simeq 1.1.$$

The distribution of kinetic energy was such that about 90% of the energy was within the wave numbers 1–5. Now for wave numbers $\leqslant 5$ the lateral friction term is really small compared with the bottom friction term. Therefore, one can conclude that the amount of total kinetic energy would not have changed significantly even if the lateral friction had been taken into account.

A comparison between K_c and K_F reveals that K_F is consistently about 10% less than corresponding values of K_c. The major part of this discrepancy arises when the stream function is computed from the observed velocity components. When $\nabla^2\psi$ is evaluated at a point, the wind components next to that point are used. (See Appendix eq. A1). This implicitly means that the values of the stream function two grid-intervals away from the point in question have been used in order to compute the vorticity at that point and thus a kind of smoothing has been introduced.

In Table 3*b* are found the predicted values that were obtained when $K_{F\text{ob}}$ (260.4) was inserted in (12b) as the initial amount of energy. We see that this analytic solution does not deviate significantly from the values of K_F in Table 3*a*. From this fact we can conclude that the finite-difference approximations in the vorticity equation have caused no violation of the total kinetic energy.

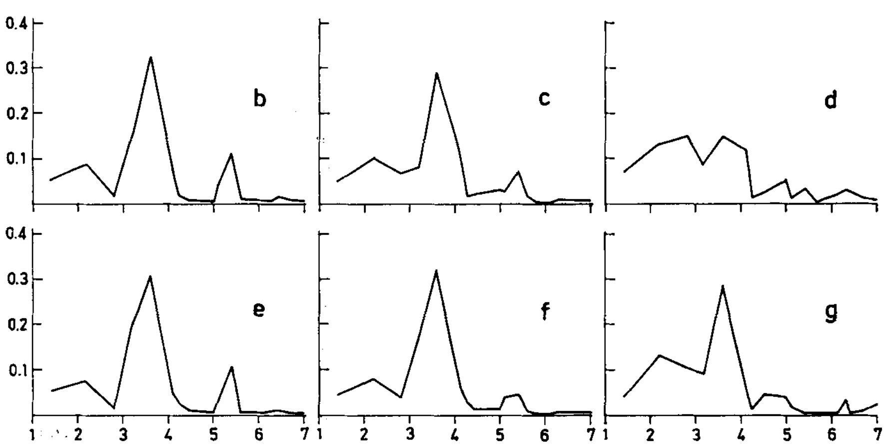

FIG. 7. (*b–g*), (*b–d*): Observed distributions of $\Sigma P_{m,n}$ for 1, 2 and 4 days respectively. (*e–g*): Predicted distributions for 1, 2 and 4 days respectively.

TABLE 4. $\sum_{m=1}^{10} \sum_{n=1}^{10} P_{mn}$.

τ	Obs.	Prog.
0	0.988	
1	0.988	0.976
2	0.988	0.967
4	0.988	0.955

The good agreement between observed and predicted total kinetic energy indicates that the way in which the bottom friction is treated is very satisfactory.

In order to represent the energy distribution in the spectrum by one-dimensional graphs the components were summed up in the following way:

The summation $\sum P_{mn}$ is taken over all m and n for which $m^2+n^2=$const. That is to say all of those components for which the wave number vector has the same magnitude are added together. The resulting curves are shown in Figs. 7*a*–7*f*. It is seen that the non-linear interactions are well predicted over one day. After two days the observed and predicted energy distributions are somewhat different and after four days this difference becomes very marked. The high values for the wave-numbers $\sqrt{10}$ and $\sqrt{13}$ in Figs. 7*f* and 7*g* are probably mainly due to neglecting z_g, which caused a too-slow damping of the motion. As was seen in Fig. 4 it was this discrepancy which was most pronounced in the lows, which have a scale corresponding to wave-number three.

The observed and forecast values of $\sum_{m=1}^{10} \sum_{n=1}^{10} P_{mn}$ are shown in Table 4. It is seen that in the forecasts there has been a systematic net flow of energy from the wave-number range 1–10 to the range 11–19. Further, however, one sees that this net flow is not verified by the observations. From the ratio (14) it is found that for wave-numbers >10 the effect of lateral friction starts to be as important as the effect of bottom friction. Thus the differences between observed and prognostic values in Table 4 would certainly have been smaller if the lateral friction had been included in the vorticity equation. However, the differences are so small that it is not feasible to estimate numerically how great a part of the deviations the omission of lateral friction is responsible for. In the next section it will be shown that the finite differences also may—at least in part—be responsible for the observed differences.

5. A study of the finite-difference approximations regarding the non-linear interactions

At first a theoretical investigation of the problem is made and then the results of a numerical experiment are presented. Finally, a discussion of how this phenomenon may give rise to computational instability is given.

Theoretical discussion

Since the study concerns only the non-linear interactions we consider the simplest vorticity equation for this purpose:

$$\frac{\partial}{\partial t}\nabla^2\psi = -J(\psi, \nabla^2\psi). \tag{15}$$

Further we apply the Fourier expansion

$$\psi = \sum_k B_k e^{i\mathbf{k}\cdot\mathbf{r}}$$

where $\mathbf{k}$ is the wave-number vector. After inserting this expansion in (15), and utilizing orthogonality properties we find

$$\frac{d}{dt}B_k = \frac{1}{k^2}\sum_{k'}(k_x k'_y - k'_x k_y)\, k'^2 B_{k'} B_{k-k'}. \tag{16}$$

With the help of (16) we now derive an equation for the rate of change of the kinetic energy. The kinetic energy in wave-number k is proportional to $k^2|B_k|^2$. (The proportionality factor is of no importance to this discussion and is thus omitted for the sake of brevity.) The coefficient B_{-k} is the complex conjugate of B_k and hence

$$\frac{d}{dt}|B_k|^2 = B_{-k}\frac{d}{dt}B_k + B_k\frac{d}{dt}B_{-k}.$$

Substituting in (16) gives

$$k^2\frac{d}{dt}|B_k|^2 = \sum_{k'}(k_x k'_y - k'_x k_y)\, k'^2 B_{k'}(B_{k-k'}B_{-k} - B_{-k-k'}B_k). \tag{17}$$

Let us now look at the change in short-wave components as it depends on the long waves. Thus we are considering $k' < k$ and summing only over a narrow range of k'. For large k's it seems reasonable to assume that the amplitudes are rather smoothly distributed. As a consequence of this assumption we have

$$B_{k-k'} \simeq B_k \quad \text{and} \quad B_{-k-k'} \simeq B_{-k}.$$

Substituting these relations in (17) we see that the right hand side of the equation becomes approximately zero. This means that the changes in the high wave-number components are not, or at least to a very little extent, directly affected by the low wave-number components. The transfer of kinetic energy from the long waves to the short waves accordingly occurs almost entirely through the intermediate scales (PEDLOSKY, 1962).

Let us now go back and start again from equation (15). But this time we approximate all derivatives by finite differences in the way this is commonly done in treating the vorticity equation. Hence we now write

$$\psi = \sum_k B_k e^{i\mathbf{k}\cdot\mathbf{p}\Delta s}$$

where $\mathbf{p}\Delta s = \mathbf{r}$; the components of $\mathbf{p}$ being integers.

The equation corresponding to (16) is then found to be:

$$\frac{d}{dt} B_k = \frac{1}{C_k (\Delta s)^2} \sum_{k'} \{[\sin (k_x - k_x') \Delta s \cdot \sin k_y' \Delta s - \sin (k_y - k_y') \Delta s \cdot \sin k_x' \Delta s] C_{k'} B_{k-k'} B_{k'}\}. \quad (18)$$

C_k is an abbreviation for

$$(2 - \cos k_x \Delta s - \cos k_y \Delta s).$$

We can check that this derivation is correct by taking the limit of (18) as Δs goes to zero and note that equation (16) results.

The forecasting equation for the kinetic energy is obtained in the same way as equation (17). One finds:

$$C_k \frac{d}{dt} |B_k|^2 = \frac{1}{(\Delta s)^2} \sum_{k'} B_{k'} C_{k'} \times \{[\sin (k_x - k_x') \Delta s \cdot \sin k_y' \Delta s - \sin (k_y - k_y') \Delta s \cdot \sin k_x' \Delta s] B_{k-k'} B_{-k} - [\sin(k_x + k_x') \Delta s \cdot \sin k_y' \Delta s - \sin(k_y + k_y') \Delta s \cdot \sin k_x' \Delta s] B_{-k-k'} B_k\}. \quad (19)$$

Again we consider the case $k' < k$. The assumption about the smoothness of the amplitude distribution may also be written in the following way:

$$B_{k-k'} \cdot B_{-k} \simeq B_{-k-k'} \cdot B_k \simeq |B_k|^2.$$

This product can be taken outside the curled brackets in (19) leaving only trigonometric functions inside. Writing $\sin(\alpha - \beta)$ as $(\sin\alpha \cdot \cos\beta - \cos\alpha \cdot \sin\beta)$ the equation (19) reduces in this case ($k' < k$) to

$$C_k \cdot \frac{d}{dt} |B_k|^2 = \frac{2}{(\Delta s)^2} |B_k|^2 \cdot [\cos k_y \Delta s - \cos k_x \Delta s] \times \sum_{k'} B_{k'} c_{k'} \sin k_x' \Delta s \cdot \sin k_y' \Delta s. \quad (20)$$

which is equal to zero *only* when $k_x = k_y$ (isotropy). That is, the right-hand side of this equation does not necessarily become zero, even if it is exactly zero in equation (17) for the case $k' < k$

Thus we see that the probability for the long waves to influence the changes of the short waves directly is greater in the case of finite-difference approximations than in reality.

However, nothing has so far been said about the sign of the right hand side of equation (20) and the equation itself does not show that there is any predominance of plus over minus or vice versa. We, therefore, carry through the following qualitative discussion. Suppose that the $B_{k'}$'s are such that the right side of (20) is negative for, say, $k_x < k_y$; then it is positive for $k_x > k_y$ because $|\mathbf{k}|$ is constant and there is a minus sign between the two cosine terms in (20). We see that this means an exponential decrease of kinetic energy in the region of the short waves where $k_x < k_y$, while where $k_x > k_y$ there will be an exponential increase of energy. Now the $B_{k'}$'s are the large scale components and these are usually very persistent. Thus we may expect the sign of the sum in (20) to be the same for a very long time during a forecast. It is quite plausible therefore to assume that *the net result will be an increase of kinetic energy in the high wave number range.*

It should be pointed out that this occurrence in itself has nothing to do with any sort of instability. It is only a redistribution of the *existing* kinetic energy; *the energy in the short waves grows at the expense of the energy in the long waves.*

If we go back and consider the differences (shown in Table 4) between observed and predicted distributions we notice that these differences can also be explained by the conclusion stated above.

A numerical example

For experimental verification and evaluation of the conclusion there was produced a field of motion to serve as an initial field for predictions. This field was composed of the three components $B_{1,1}$, $B_{3,2}$ and $B_{6,9}$ which were chosen so that they contained respectively 29%, 67% and 4% of the total kinetic energy. The stream function was computed with the aid of (7). A sketch of its initial pattern is shown in Fig. 8.

Since the initial field was artificially produced there were no observations available for verification of the forecasts. Instead, the forecasts were prepared three times according to (15) with a different grid-interval at each time. In addition, a forecast of the Fourier components was made, according to equation (8) with $D=0$.

The grid distances used were

$$(\Delta s)_1 = \frac{L}{20}, \quad (\Delta s)_2 = \frac{L}{14}, \quad (\Delta s)_3 = \frac{L}{10}.$$

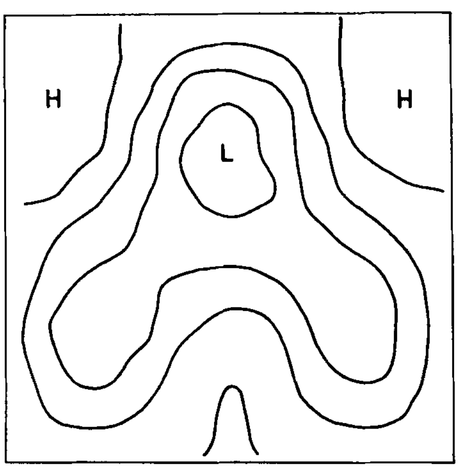

FIG. 8. A sketch of the constructed initial stream pattern.

In equation (8) N was set equal to 10, which thus corresponds to the $(\Delta s)_3$ case. From the choice of the amplitudes we now further see that for the case $(\Delta s)_1$ there was initially no energy at all in wave lengths $\leqslant 4\Delta s$ while in both $(\Delta s)_2$ and $(\Delta s)_3$ 4% of the total energy was in wave lengths $\leqslant 4\Delta s$.

In the $(\Delta s)_1$ and $(\Delta s)_2$ cases the same time-step was used and the forecasts were printed out after 10, 20 and 30 steps. These three points in time are referred to as I, II and III respectively. In the $(\Delta s)_3$ case and for the component-forecast the time-step was double that used in the other two cases.

Since the forecasting program was written in ALGOL, the double summation in equation (8) was a very time-consuming procedure. This equation was therefore integrated only up to time I.

In Table 5 the sum $\sum_{m=1}^{M} \sum_{n=1}^{M} P_{mn}$ is shown. M gradually increases up to the value $N-1$ which is applicable to the grid distance in question. We see that the energy in wave number (3; 2) is spreading out both to both longer and shorter waves (FJÖRTOFT, 1953). The increase of energy in the longest waves has been predicted almost identically by all the different approximations while the transfer of energy between the long waves and the short waves has been variously forecast as the different grid-sizes were used. *It is very evident that an increase of the grid-interval is associated with an increased net flow of energy from the longer waves to the shortest waves in the spectrum.* The differences increase with increasing time. At time III, however, there is a somewhat higher value for $M=3$ in $(\Delta s)_3$ case than in the $(\Delta s)_2$. The phenomenon that we are considering may, however, have become obscured by other effects (e.g. feed-back) through the crudeness of the $(\Delta s)_3$ approximation.

It was said above that the truncated Fourier series used corresponds to the $(\Delta s)_3$ case with regard to the wave lengths which may be represented. *The Fourier expansion, however, implies that the space derivatives are evaluated exactly and it is seen that there is a marked tendency to retain the energy in the long waves.* Of course, there would have been a somewhat different distribution if the Fourier expansion had covered more wave-numbers. Essential changes in the present values, though, would probably only appear for $M=7$ and 9 because

TABLE 5. $\sum_{m=1}^{M}\sum_{n=1}^{M} P_{mn}$.

The bottom row gives the percental change of the initial total kinetic energy.

	Initial Δs...	I				II			III		
M	All cases	$(\Delta s)_1$	$(\Delta s)_2$	$(\Delta s)_3$	Prog. of F comp.	$(\Delta s)_1$	$(\Delta s)_2$	$(\Delta s)_3$	$(\Delta s)_1$	(Δs_2)	$(\Delta s)_3$
1	0.287	0.289	0.289	0.298	0.293	0.300	0.304	0.320	0.320	0.327	0.322
2	0.287	0.293	0.295	0.311	0.298	0.312	0.325	0.341	0.346	0.358	0.344
3	0.958	0.904	0.855	0.720	0.913	0.807	0.681	0.511	0.687	0.541	0.578
5	0.958	0.937	0.919	0.910	0.946	0.916	0.874	0.888	0.885	0.821	0.788
7	0.958	0.941	0.924	0.922	0.952	0.924	0.887	0.941	0.903	0.876	0.915
9	1.000	0.963	0.949	1.000	1.000	0.935	0.905	1.000	0.921	0.916	1.000
13	1.000	0.997	1.000			0.975	1.000		0.958	1.000	
19	1.000	1.000				1.000			1.000		
		−0.7	+0.7	+1.3	+0.9	+0.8	+4.7	+8.9	+2.4	+5.8	+9.2

the transfer occurs, for the most part, through the intermediate scales.

There is still another notable fact that becomes clear from Table 5; namely, that the amount of energy spuriously transferred from the low to the high wave-numbers is squeezed into the highest wave-number of the spectrum in question. For example, at time I, there is less than 4% of the energy in the range 10 to 19 (case $(\Delta s)_1$) while there is more than 5% of the energy in the range 10 to 13 (case $(\Delta s)_2$); in the case of the forecast of Fourier components there is 5% while in $(\Delta s)_3$ case there is 8% of the energy in the range 8 to 9. This fact can be seen at all three times.

The results obtained in this numerical example are such that they do confirm the conclusion made above.

The spurious flow of energy as a source of computational instability

PHILLIPS (1959) discussed a kind of computational instability due to the grid system misrepresenting the non-linear interactions between high wave-number components (wavelengths $<4\Delta s$). The misrepresentation implies that a long-wave component is affected, when in reality it is a short-wave component that should be influenced by the nonlinear interaction. This component that should be affected has, however, such a high wave-number that it cannot be represented by the grid (e.g. $P>N$). Instead wave-number $(2N-P)$ is affected.

We have seen that the finite-difference approximations cause an increase in the amplitudes of the shortest waves in the spectrum. These short-wave amplitudes may then eventually become so large that the $(2N-P)$ components start to grow significantly due to the kind of instability briefly described above.

In the same investigation Phillips presents a numerical example containing instability which, however, was removed by introducing a smoothing procedure in the computations. This smoothing was performed by periodically removing all waves of a length $<4\Delta s$ from the field of motion. This means that the transfer of energy from the long waves *directly* to the short ones (which the finite differences permit) is effectively prevented. Hence, the fictitious increase of energy in the shortest waves is postponed until energy reaches these waves through the intermediate scales. If a smoothing of this type is adopted in the computations it probably has to be performed frequently, so that not too much energy has had the opportunity to reach the band to be cut off, which would mean that too much energy could be taken away from the system.

Conclusions

On the basis of the preceding considerations one may draw the following conclusions. The finite-difference approximations of the space derivatives implies that the *direct* transfer of energy from the long waves to the shortest waves of the spectrum occurs considerably easier in a numerical forecast than in reality. The result of this spurious transfer is that too much energy will be moved over from the long waves to the short ones. This effect is reduced when the grid increment is made smaller.

It seems desirable to choose the grid interval so small that the energy content in the wave lengths $<4\Delta s$ is only a few per cent of the total energy of the initial field. Then the distortion of the energy distribution probably does not become serious in a short-term forecast.

However, when a prediction is extended over a long period, the increase of energy in the high wave-numbers may give rise to computational instability. Therefore, it is justified to smooth the field by periodically eliminating all scales $<4\Delta s$. This procedure effectively breaks the fictitious flow of energy to the shortest waves of the spectrum and in consequence of this the computational instability is prevented.

The spectral distribution of kinetic energy becomes certainly better predicted by forecasting the Fourier components of the motion field than by conventional methods. This fact makes the component forecasting attractive. The very fast machines that are available will undoubtedly reduce the computation time so much that the forecasts become practically useful. However, there are many other things (e.g. simplifying assumptions in the basic equations) that affect the accuracy of a forecast more than the finite-difference approximations do. Thus it is questionable if the accuracy gained when Fourier components are forecast is worth the extra expense which will come beyond the costs of the ordinary forecasting.

Acknowledgments

I wish to express my sincere thanks to Dr. A. Faller of the Woods Hole Oceanographic Institution who suggested this project and together with whom it was begun. Dr. Faller conducted the tank experiments and made specific suggestions for the method of analysis of data and for the investigation of observational errors. Thanks are also due to Mr. J. Pedlosky of Massachusetts Institute of Technology for valuable discussions in connection with the study of the nonlinear transfers.

Appendix

Some comments on the methods of computation

The stream function was computed from the velocity components according to the finite-difference equation (written in the notations commonly used)

$$\nabla^2 \psi = \frac{\Delta s}{2}[v_{i+1,j} - v_{i-1,j} - u_{i,j+1} + u_{i,j-1}]. \qquad \text{(A 1)}$$

Equation (A 1) and the prognostic equations were solved by the method of Liebmann relaxation. (See THOMPSON, 1961.)

The time derivative was approximated in the usual way

$$\frac{\partial \zeta}{\partial t} \simeq \frac{1}{2\Delta t}[\zeta^{\tau+1} - \zeta^{\tau-1}]; \left(\tau = \frac{t}{\Delta t}\right).$$

In order to assure computational stability the friction term was given the mean value $\frac{1}{2}D$ $(\zeta^{\tau+1} + \zeta^{\tau-1})$, (PHILLIPS, 1960) and the criterion on the time-step becomes:

$$\Delta t < \frac{\Delta s}{\sqrt{2U_{\max}^2 + (D \cdot \Delta s)^2}}.$$

For $D = 0$ we obtain the Courant-Friedrichs-Lewy condition (CHARNEY, FJÖRTOFT and VON NEUMAN, 1950).

In order to suppress possible exponential growth at the start of the time integration the first step was taken over $\frac{1}{4}\Delta t$ as suggested by GATES (1960). Then the succeeding steps were taken according to the centered method. The starting procedure is visualized in Fig. A 1.

Introduction of additional observational errors

We put

p_0 = original observational error,
p_1 = errors that should be introduced.

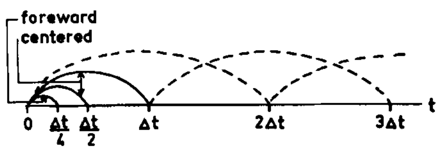

FIG. A1. Principles of the time integration. Full lines show the starting process. Dashed lines give the ordinary centered procedure.

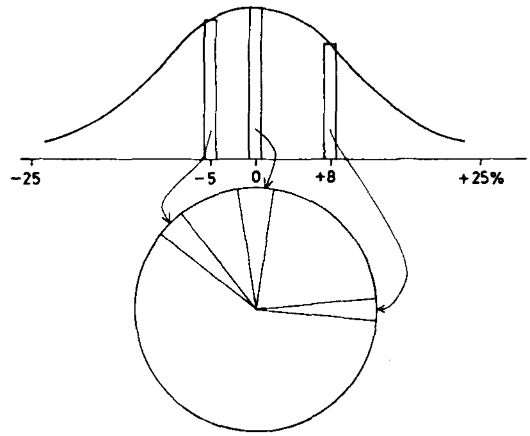

FIG. A2. Sketch showing the principles of the device used to randomly introduce additional observational errors.

Now we want to get an error in the new fields twice the original error. Hence

$$\overline{(p_0+p_1)^2} = \overline{(2p_0)^2}.$$

Assuming that there is no correlation between p_0 and p_1 we find

$$\overline{p_1^2} = 3\overline{p_0^2}.$$

Thus having the standard deviation of p_1 we also know its normal distribution. The area under the normal curve from -25% to $+25\%$ was assumed to be represented by a circular area. The circular sectors were drawn proportional to the frequence area under the normal curve for each integer between -25 and $+25$. Fig. A2 shows the principles of this method. With the aid of this "roulette" the errors were randomly introduced into the velocity fields.

REFERENCES

BOLIN, B., 1955, Numerical forecasting with the barotropic model. *Tellus*, **7**, pp. 27–49.

BOLIN, B., 1956, An improved barotropic model and some aspects of using the balance equation for three-dimensional flow. *Tellus*, **8**, pp. 61–75.

CHARNEY, J. G., and ELIASSEN, A., 1949, A numerical method for predicting the perturbations of the middle latitude westerlies. *Tellus*, **I**, **2**, pp. 38–54.

CHARNEY, J. G., FJÖRTOFT, R., and VON NEUMAN, J., 1950, Numerical integration of the barotropic vorticity equation. *Tellus*, **2**, pp. 237–254.

EKMAN, V. W., 1905, On the influence of the earth's rotation on ocean currents. *Arkiv f. Matem., Astr. o. Fysik*, Stockholm, **2**, No. 11, 53 pp.

FJÖRTOFT, R., 1953, On the changes in the spectral distribution of kinetic energy for two-dimensional, nondivergent flow. *Tellus*, **5**, pp. 225–230.

GATES, W. L., 1960, Note on suppression of the oscillation in numerical integration. *J. Met.*, **197**, pp. 572–574.

LORENZ, E. N., 1960, Maximum simplification of the dynamic equations. *Tellus*, **8**, pp. 243–254.

PEDLOSKY, J., 1962, Spectral considerations in two-dimensional incompressible flow. *Tellus*, **2**, pp. 125–132.

PHILLIPS, N. A., 1959, An example of non-linear computational instability. *The Rossby Memorial Volume*. Rockefeller Institute Press, New York, pp. 501–504.

PHILLIPS, N. A., 1960, Numerical weather prediction ALT, F. C. *Advances in Computers*, Vol. 1, pp. 43–90.

SALTZMAN, B., 1959, On the maintenance of the large scale quasipermanent disturbances in the atmosphere. *Tellus*, **4**, pp. 425–431.

THOMPSON, P. D., 1961, *Numerical Weather Prediction*, Ch. 8. Macmillian Comp., New York.